sustainability

MDPI

Article

Predicting the Degree of Reaction of Supplementary Cementitious Materials in Hydrated Portland Cement

Aron Berhanu Degefa [1], Seunghee Park [2], Beomjoo Yang [3,*] and Solmoi Park [1,*]

[1] Department of Civil Engineering, Pukyong National University, 45 Yongso-ro, Nam-gu, Busan 48513, Republic of Korea; aaronpknu@pukyong.ac.kr
[2] School of Civil, Architectural Engineering& Landscape Architecture, Sungkyunkwan University, Suwon 16419, Republic of Korea; shparkpc@skku.edu
[3] School of Civil Engineering, Chungbuk National University, 1 Chungdae-ro, Seowon-gu, Cheongju 28644, Republic of Korea
* Correspondence: byang@chungbuk.ac.kr (B.Y.); solmoi.park@pknu.ac.kr (S.P.)

Abstract: Determination and prediction of degree of reaction (DOR) of supplementary cementitious materials (SCMs) in hydrated Portland cement are important for designing concrete with lower levels of embodied carbon dioxide. Herein, a model for predicting the DOR of SCMs in hydrated cement was developed using a set of collected data and a machine learning algorithm based on genetic programming toolbox for the identification of physical systems. The results suggest that the model reliably predicts the DOR of slag, fly ash, metakaolin, and silica fume with a coefficient of determination (R^2) value of 0.89. The predicted DOR of SCMs is found to be directly proportional to water-to-cement ratio and curing time, while it is highly reliant on the oxide composition and differs amongst SCMs. For instance, the DOR of slag substantially increased with a higher alumina content, while the DOR of metakaolin remained more stable, primarily influenced by the silica-to-alumina ratio. The proposed model is particularly useful for predicting phase assemblages of SCMs-blended Portland cement when experimental data and information on SCMs are limited and properties of SCMs are highly variable. The insights gained from this study offer a pathway towards more sustainable and efficient concrete design, aligning with contemporary environmental objectives.

Keywords: supplementary cementitious materials; degree of reaction; machine learning; prediction; thermodynamic modeling

Citation: Degefa, A.B.; Park, S.; Yang, B.; Park, S. Predicting the Degree of Reaction of Supplementary Cementitious Materials in Hydrated Portland Cement. *Sustainability* **2023**, *15*, 15471. https://doi.org/10.3390/su152115471

Academic Editors: Yao Sun, Luigi Di Sarno and Oliver Kinnane

Received: 12 September 2023
Revised: 23 October 2023
Accepted: 25 October 2023
Published: 31 October 2023

1. Introduction

Concrete is the world's second most utilized material, behind water [1]. Unfortunately, being a primary component of concrete, cement production is not environmentally friendly, since it requires a significant amount of energy, which results in the emission of massive amounts of anthropogenic CO_2. Currently, the cement industry accounts for approximately 8% of global CO_2 emissions [2]. As a result, the cement industry was actively developing plans and policies to ensure acceptable carbon emissions. China, the world's top cement manufacturer, user, and CO_2 emitter, pledged that by 2030, GDP CO_2 emissions per capita would be 60–65% lower than in 2005 [3]. In 2009, the IEA roadmap proposed an 18% reduction in CO_2 emissions from the cement sector by 2050 compared to 2006 [4]. To stay on track with the IEA plan, an annual reduction of 3% in CO_2 emissions is required beginning in 2020 and continuing until 2030 [5]. Hence, technologies that mitigate CO_2 emissions and reduce the CO_2 footprint of concrete are urgently demanded. These include the use of supplementary cementitious materials (SCMs), cements made of alternative clinkers, carbon capture, utilization and storage techniques, alkali-activated cements, and improving the efficiency of cement use and structural solutions [1,6]. Among these, SCMs are the most favorable carbon reduction alternative due to the past accumulated experimentations,

which provide a foundation for further research, as well as their reduced cost and good performance [7,8].

SCMs are clinker-replacement materials that can provide extra silicates, aluminosilicates, or calcium aluminosilicates that can react to form different hydration products. SCMs can improve the properties of cementitious systems by exhibiting pozzolanic properties, hydraulic properties, or filler properties [9]. The major SCMs used recently are slag, fly ash, limestone, calcined clays (metakaolin), and silica fume, with plenty of research data available. Currently, slag, fly ash, and limestone account for the vast majority of mineral additions. However, because of its extensive use and the ever-growing effectiveness in steel-making technology, slag availability is declining, leaving limited room for future CO_2 reduction [1]. Fly ash, on the other hand, is twice as abundant as slag, but due to its variable quality, only about one-third is suitable for replacement [10]. Limestone can be used in Portland cement (PC) up to a maximum of 15% and must be ground to a specific level of fineness; however, using more than this percentage will result in poor strength and porosity [11]. Silica fume availability is very low and usually preferred for the production of high-strength concrete [10]. Calcined clays represent the ideal alternative for cement replacement due to their abundance, even more so than cement, and can be utilized as a cement substitute with comparable performance [12]. However, direct measurement of SCMs performance is challenging because it is difficult to determine which way or combination of ways the SCMs altered the cementitious material property, which indirectly implies the DOR.

Numerous methods have been proposed for determining DOR, but they often lack certain requirements. For instance, some of these methods are only applicable to specific SCMs, pose issues regarding precision and replication, are laborious and time-consuming, and do not consider latent hydraulic properties. A detailed overview of the various DOR determination methods, along with their respective shortcomings, is provided in Table 1. The choice of a DOR determination method depends on the properties of the material and the required level of analytical precision. This highlights the critical importance of selecting a suitable DOR assessment method that aligns with the objectives of the study and the attributes of the material. Table 1 also underscores the necessity for alternative approaches to DOR determination, as many existing methods have limitations. On the contrary, there are some in-depth characterization approaches, notably those related to nano-size imaging, which provide great possibilities for determining DOR in the future using structure-property connections but are still in their early stages [13]. Moreover, machine learning algorithms can be utilized effectively to predict the DOR. Machine learning is used to create algorithms that can take in input data and then use statistical analysis to estimate the output depending on the type of data available [14]. Machine learning has demonstrated its effectiveness in enhancing predictive accuracy and reliability, especially in challenging scenarios involving the inherent complexity of cementitious materials, despite the existence of various methods for DOR determination [15–17]. DOR prediction can be aided by machine learning, especially when experimentally obtained results show large variability, characterization is difficult, new material has been produced, and time is constrained.

The accurate prediction of the DOR of SCMs using machine learning models can significantly enhance their adoption and utilization, thereby supporting sustainable construction practices. SCMs foster sustainability in construction in multiple ways. Rahla et al. [18] thoroughly demonstrated the advantages of incorporating SCMs such as slag, fly ash, and silica fume regarding their environmental impact, economic performance, and functional benefits as with their aggregated sustainability score. Furthermore, SCMs play a pivotal role in natural resource utilization by promoting efficient resource usage through waste material recycling, ultimately producing cost-effective concrete [19,20]. Additionally, SCMs have the potential to significantly enhance the properties of cementitious systems through a synergistic effect, resulting in improved strength and durability [21,22]. Moreover, their utilization leads to energy savings during production. Siddika et al. [23]

demonstrated that using rice husk ash as an SCM produces energy-efficient concrete with reduced energy consumption.

The present study aims to produce a model that can predict the DOR of the SCMs from their main properties using machine learning. Concerning the data obtained, a machine learning algorithm based on GPTIPS appears to best interpret the data [24]. The findings indicate that the results correlate well with the laboratory DOR. Accordingly, by incorporating the results of the DOR model into the inputs of thermodynamic modeling software, the phase assemblage outputs of the SCMs in hydrated PC were predicted.

Table 1. Common DOR determination methods and their limitations.

DOR Tests	Description	Limitations	References
Selective dissolution	The unreacted clinker phases, as well as the hydrates from the clinker and SCMs, are dissolved, leaving just the unreacted SCM as a residue for quantification	• Dissolution is incomplete, leading to large non-quantifiable errors • Various assumptions are made that are challenging to replicate in different laboratories. • There are hydrated phases that are non-dissolvable • Used for slag and fly ash only	[25–27]
XRD (Rietveld-PONKCS)	Quantification of amorphous and crystalline phases using diffraction data	• Results cannot be reproduced between laboratories due to differences in the refining process • Precision becomes poor below 10% SCM replacement • The variation in C-S-H crystallinity in regular OPC hydration and UHPC can lead to errors in C-S-H quantification.	[28,29]
SEM-BSE	Determination of element composition by forming a relation between image brightness and atomic number	• It is challenging to quantify fine (small) particles • A limited number of high-resolution SEMs and technology is still developing • laborious and time-consuming	[25,30,31]
NMR	Determination of composition, local structure ordering, and bonding from resonance frequencies that are determined by the gyromagnetic ratio of the nucleus, the magnetic shielding interaction and the quadrupolar interaction, peak multiplicities that are generated by the scalar couplings to neighboring nuclei, and peak intensities.	• Cannot be utilized for materials having substantial amounts of paramagnetic ions, such as iron • Sensitivity is low and needs at least micromolar amounts of material for analysis • Limited experience and equipment availability • Time-consuming	[7,27,32,33]
Chapelle's test	Quantification of consumed portlandite from ($Ca(OH)_2$) reaction with pozzolan	• Quantifications need to be adjusted according to the amorphous content • Does not take into account materials' latent hydraulic properties • Correction for carbonation is required since preventing it is impracticable	[7,34–36]

Table 1. *Cont.*

DOR Tests	Description	Limitations	References
Frattini test	Chemical titration to quantify the amounts of dissolved Ca^{2+} and OH^- in a cement and pozzolan solution.	• Does not take into account materials' latent hydraulic properties • $Ca(OH)_2$ solubility data are determined for OH- concentrations only ranging from 35 to 90 mmol/L	[7,36–38]
Saturated lime method	Similar to the Frattini test but a saturated lime solution is mixed with a pozzolan to determine amounts of dissolved Ca^{2+} and OH^-	• Does not take into account materials' latent hydraulic properties • The activator to pozzolan ratio is very low • Variation in the absolute quantity of $Ca(OH)_2$ in each sample might lead to errors	[37,39]
Strength activity index	Relation derived from mortar compressive strength containing cement and pozzolan	• It makes no distinction between whether the strength is derived from filler (inert) material and physical packing or chemical reactivity • It takes a longer time (28–90 days)	[7,37,39]
Bulk resistivity index test	Relation derived from mortar bulk resistivity containing cement and pozzolan	• External conditions such as curing temperature and sample saturation have a significant impact on the results, which must be thoroughly investigated	[40]
R3 test (heat release and bound water methods)	A paste prepared from the major components (SCM and portlandite) with calcite and sulfate is investigated for released heat until seven days, and bound water is assessed for 7-day cured samples that are heated at 350 °C for 2 h	• It is not suitable for slowly reacting materials having limited reactivity at seven days • It is difficult to distinguish between latent hydraulic and pozzolanic materials	[40,41]
Modified R3 test	The heat release of a KOH solution containing calcium hydroxide and SCM is measured until ten days, and additionally, TGA is performed on the resulting blends after 240 h	• It is not suitable for slowly reacting materials having limited reactivity at ten days • Should be verified by comparing it to established techniques for assessing SCM reactivity	[41]

2. Methods

This section outlines the methodology employed to analyze and predict the DOR of SCMs. The methodology encompasses two key aspects: Machine Learning prediction and its application through thermodynamic modeling. The initial phase involves collecting a comprehensive dataset, which undergoes pre-processing before machine learning predictions. This pre-processing includes several steps, such as data cleaning, imputation of missing values, and normalization of numerical features. These steps ensure that the subsequent machine-learning-based regression analysis is built on a robust and reliable foundation, optimizing the accuracy and effectiveness of the predictive model. The next phase involves determining the application of the model using thermodynamic modeling to estimate phase outputs of Portland cement blended with SCMs, enabling a comprehensive understanding of the hydration and dissolution processes. Subsequent sections delve into the specific methodologies and techniques used in greater detail.

2.1. Data Collection and Machine Learning Algorithm

A set of data was collected having the main inputs as oxide compositions of PC and SCMs, water-to-cement (w/c) ratio, curing temperature, curing time, surface area, the proportion of PC and SCMs, and experimental DOR. The DOR of the SCMs was determined through various experimental methods, including selective dissolution, quantitative X-ray Diffraction (QXRD), Scanning Electron Microscope—Backscattered Electron Imaging (SEM-BSE), and Nuclear Magnetic Resonance (NMR). For instance, Ben Haha et al. [25] demonstrated the use of BSE for determining the DOR, whereas Narmluk and Nawa [42] employed selective dissolution to determine the DOR. The collected data had 254 observations, 20 independent variables, and DOR as a dependent variable. A machine-learning-based regression analysis was used to predict the DOR. For this research, an open-source multi-gene genetic programming (MGGP) for data mining and model discovery, also known as GPTIPS, was used [43]. The GPTIPS is a genetic programming (GP) that is a classical machine learning method inspired by biology [24]. The main feature of GPTIPS, compared to traditional GP, uses a symbolic multi-gene regression (SMGR) for data analysis that discovers non-linear correlations between input and output data.

The processes of the data-driven model in the form of symbols can be recapitulated as follows [44]: GPTIPS initiates with a population of MGGP from randomly generated vector trees. The fitness of various solutions is evaluated, and then regular tournament selection is carried out based on a probabilistic Pareto tournament [45]. The regular tournament develops by repeating mutation and crossover up to a pre-set truncation criterion. When the analysis results reach the fitness function, it creates symbolic formulas to describe the overall characteristics of chemical systems. It is worth noting that the GPTIPS deeply analyzes the user-defined input variables and output, identifies the most influential key variables, and excludes the redundant input variables [46]. Following the development of a model to predict the DOR, its accuracy was compared to experimental data, as well as its relationship to the main inputs such as w/c ratio, curing temperature, curing time, and oxide composition of the SCMs. The correlations were established by inserting different values for the main inputs and assessing the resulting variations in DOR. For instance, the W/C ratio varied from 0.2 to 0.8, and curing time ranged from the 28th day to the 360th day.

2.2. Thermodynamic Modeling

Thermodynamic modeling was used to estimate the phase outputs of PC blended with the SCMs. The program GEM-Selektor v.3 (http://gems.web.psi.ch/GEMS3/ (accessed on 1 December 2021)) was used to perform the modeling [47,48]. Cemdata18, the most recent database, was added to the software's default database for modeling [49]. The extended Debye-Hückel equation was used to calculate activity coefficients for aqueous species. Because it was assumed that KOH dominated the aqueous phase, the common ion size parameter and short-range interaction parameter used were 3.67 Å and 0.123 kg/mol, respectively [50]. The simulated phase assemblage of PC hydration was predicted, with incremental substitution of 0–100 wt% of the SCMs. The adapted cement hydration model [51,52], which was initially developed by Parrot and Killoh (1984) [53], was used to predict the dissolution rate of PC clinker. The oxide compositions of SCMs adopted in the DOR predictions shown in Table 2 were averaged from the collected data, except for the composition of slag, which was taken from a previous article [54]. The temperature, curing time, and w/c ratios were kept at 20 °C, 180 days, and 0.4, respectively, for all simulations unless stated.

Table 2. Chemical compositions of the raw materials.

Oxides (Mass-%)	SiO_2	Al_2O_3	Fe_2O_3	CaO	MgO	SO_3	Na_2O	K_2O
PC	20.2 ± 0.12	5.6 ± 0.13	2.4 ± 0.12	65.9 ± 0.14	2.0 ± 0.05	2.6 ± 0.1	0.5 ± 0.04	0.7 ± 0.03
Slag	36.49	12.26	0	41.79	7.48	1.98	0	0
Fly ash	51.8 ± 1.12	23.4 ± 0.48	7.2 ± 0.3	10.8 ± 1.08	2.7 ± 0.22	1.1 ± 0.2	1.3 ± 0.17	1.6 ± 0.13
Metakaolin	54.1 ± 0.4	43.6 ± 0.6	1.1 ± 0.18	0.2 ± 0.03	0.2 ± 0.05	0.1 ± 0.04	0.1 ± 0.02	0.5 ± 0.09
Silica fume	99.3 ± 0.47	0.1 ± 0.05	0	0.1 ± 0.11	0.1 ± 0.09	0	0.1 ± 0.06	0.2 ± 0.15

3. Results

To measure how well the experimental outcomes are replicated by the model, two fitting criteria were used, which are the coefficient of determination (R^2) and the Pearson correlation coefficient (r) defined in Equations (1) and (2), respectively. The adjusted R^2 is not explained since it gives almost identical results as R^2. Figure 1 illustrates a comparison between the predicted degree of reaction and the experimental degree of reaction for slag, fly ash, metakaolin, and silica fume. The close alignment observed between the experimental and predicted degrees of reaction serves to underscore the reliability and effectiveness of the predictive models utilized in this analysis. The model predicts the DOR of the supplementary cementitious materials with a minimum accuracy of 83%. The prediction results show that the model estimates the DOR of silica fume, metakaolin, slag, and fly ash in decreasing order of accuracy, whereby silica fume and metakaolin DOR are predicted with very high accuracy, as shown in Table 3.

$$R^2 = \frac{\left(\sum(Yi - Ym)^2 - \sum(Yi - Yp)^2\right)}{\sum(Yi - Ym)^2} \quad (1)$$

where Yp is the predicted value of the model, Yi is the ith value, and Ym is the mean value.

$$r = \frac{\sum((Xi - Xm) \times (Yi - Ym))}{\sqrt{\sum(Xi - Xm)^2 \times \sum(Yi - Ym)^2}} \quad (2)$$

where Xi and Yi are the ith values and Xm and Ym are the mean values.

The effect of w/c ratio on the DOR of SCMs is shown in Figure 2. A broad range of w/c ratios were employed to assess their influence on the properties of the cementitious material. This was undertaken primarily to offer a comprehensive perspective on the behavior of the material across varying w/c ratios, which is crucial for a thorough understanding of its performance. The decision to employ a high w/c ratio was based on specific considerations aimed at simulating conditions relevant to practical applications. In certain real-world scenarios, particularly in construction projects or concrete formulations, a high w/c ratio is indeed employed to achieve the desired workability, improve flow, and ensure ease of placement. This is because a higher w/c ratio makes the concrete more fluid and easier to deal with, which can be helpful when pouring concrete into intricate molds or navigating through complex constructions [55]. Moreover, this approach is often favored when time is a critical factor, as it can expedite the pouring and setting processes, allowing for more efficient progress on the construction site. Additionally, a high w/c ratio may be necessary when the SCMs used have very fine particles [56]. For all SCMs, the DOR increases with increasing w/c ratio, similar to previous studies [57,58], with the main variances arising from the SCMs replacement content. Although these variations are not directly related to the w/c ratio, they may be used to compare the DOR with the major inputs included in the model and are thus described. The DOR of slag constantly decreases when its replacement is increased. This is due to a decrease in the alkaline activating environment created by cement hydration [58]. The DOR of fly ash can be clearly described by dividing it into four zones, the first being a 0–50% replacement of PC, where the DOR falls significantly, the second replacing from 50 to 60%, where the DOR remains constant, the third from 60 to 95, where the DOR rises slightly, and finally from 95 to 100% where the DOR remains

constant. The DOR of fly ash initially demonstrates a decreasing trend, potentially due to factors such as the characteristics of the fly ash, its pozzolanic reactivity, cementitious system composition, and curing conditions. As the replacement level of fly ash increases, the available reactive compounds may become saturated, resulting in the observed decrease in DOR. However, as the replacement level continues to rise, other influencing factors come into play, such as improved dispersion of fly ash particles and extended reaction time. These factors can contribute to a subsequent increase in the degree of reaction, countering the initial decrease observed in DOR. The DOR of metakaolin slightly decreases up to 10% replacement of PC and then drops significantly up to 80% replacement, and then remains constant. The DOR of silica fume significantly drops up to 78% replacement of PC, after which it remains constant.

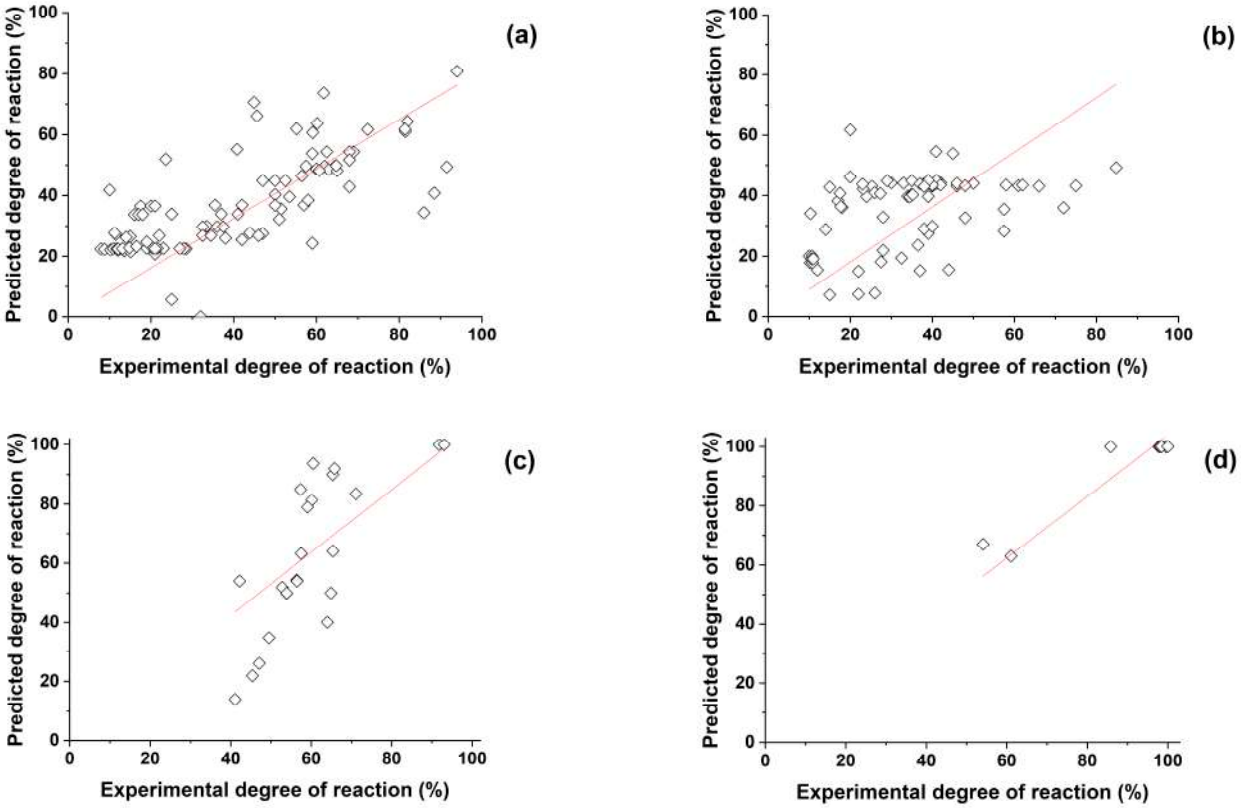

Figure 1. Predicted degree of reaction (%) vs. Experimental degree of reaction (%) of (**a**) slag, (**b**) fly ash, (**c**) metakaolin, and (**d**) silica fume (symbols and lines indicate the experimental degree of reaction and linear fit of the SCMs predicted degree of reaction, respectively).

Table 3. Model accuracy considering two different fitting criteria.

Fitting Method	Coefficient of Determination	Pearson Correlation Coefficient
Slag	88.5	94.1
Fly ash	83.6	91.4
Metakaolin	93.3	96.6
Silica fume	99.7	99.8

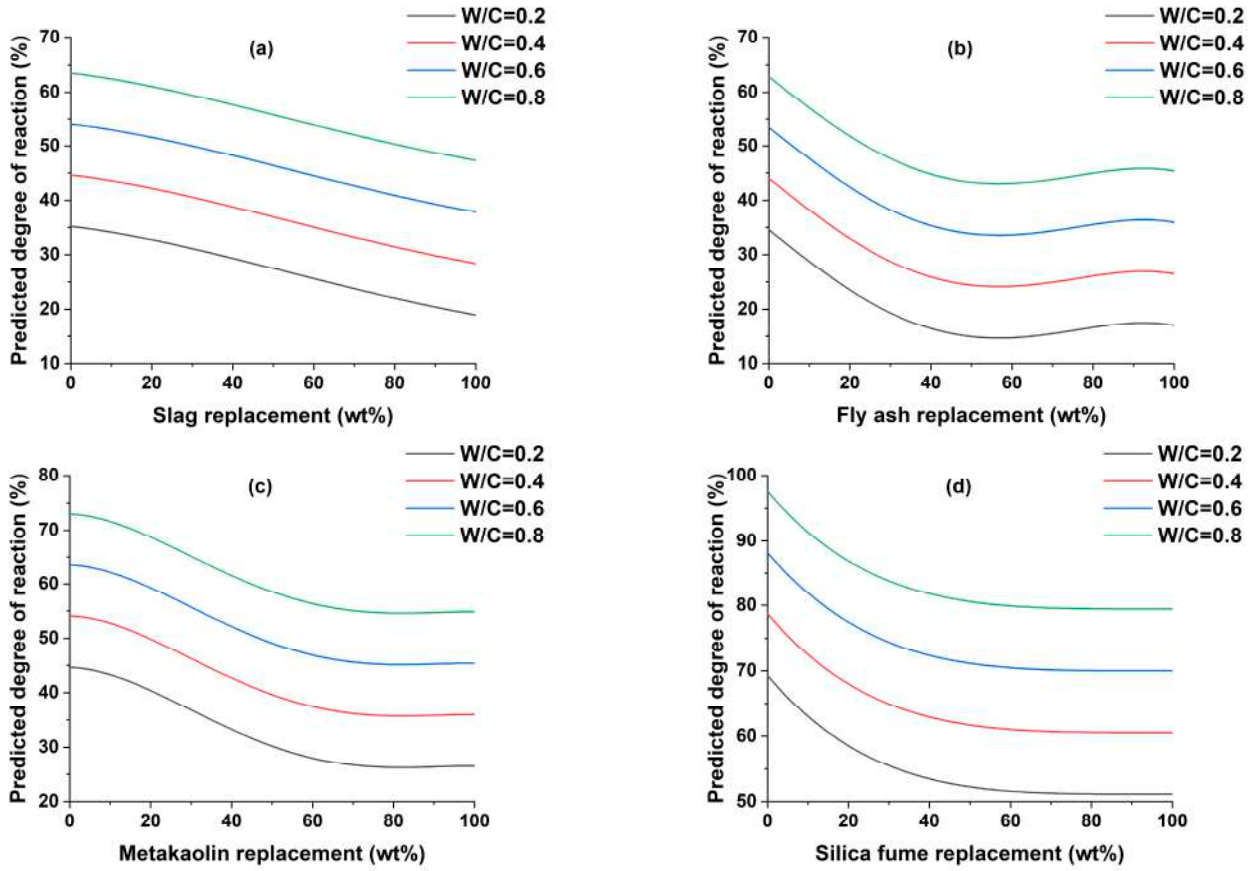

Figure 2. The effect of w/c ratio on the degree of reaction of (**a**) slag, (**b**) fly ash, (**c**) metakaolin, and (**d**) silica fume.

These trends for fly ash, metakaolin, and silica fume are best described by comparing the phase assemblage outputs computed using the DOR model since most of the replacement levels are ideal, particularly higher replacement levels, which have not yet been investigated in previous studies. It has been found that replacing cement with 30% fly ash results in the consumption of portlandite and ettringite, while promoting the formation hemicarboaluminate and monocarboaluminate [59], as similar to the simulation results. The only difference is the formation of monosulfoaluminate in place of hemicarboaluminate and monocarbolauminate due to sulfate-dominated composition of the fly ash. Additionally, increasing the fly ash replacement from 0 to 50 results in the hydration of cement, but decreases the reaction extent of fly ash due to portlandite consumption [60], which is consistent with simulation results. For metakaolin, 40% replacement results in complete consumption of portlandite, whereby its disappearance is associated with the formation of straetlingite, and as metakaolin replacement increases from 0 to 20 to 40, the amount of unreacted metakaolin and aluminum-bearing products increases [61], similar to the predicted phase assemblage. In the case of silica fume, hydrated cement without silica fume tends to consume ettringite and convert it to monosulfate, but 10% silica fume substitution can result in stabilizing ettringite at later ages [62], and Uzbas and Aydin showed that portlandite consumption increases as the amount of silica fume replacement increases from 0% to 20%, for 0%, 5%, 10%, 15%, and 20% replacements [63] both scenarios supported by the thermodynamic simulation.

The effect of the curing time on the DOR of SCMs is shown in Figure 3. For all SCMs, the DOR increases with increasing curing time, as reported by previous studies [59,62,64,65]. The variations are caused by SCMs replacement content, as previously stated, and are analogous to the variances discussed in the effect of w/c ratio on the DOR section.

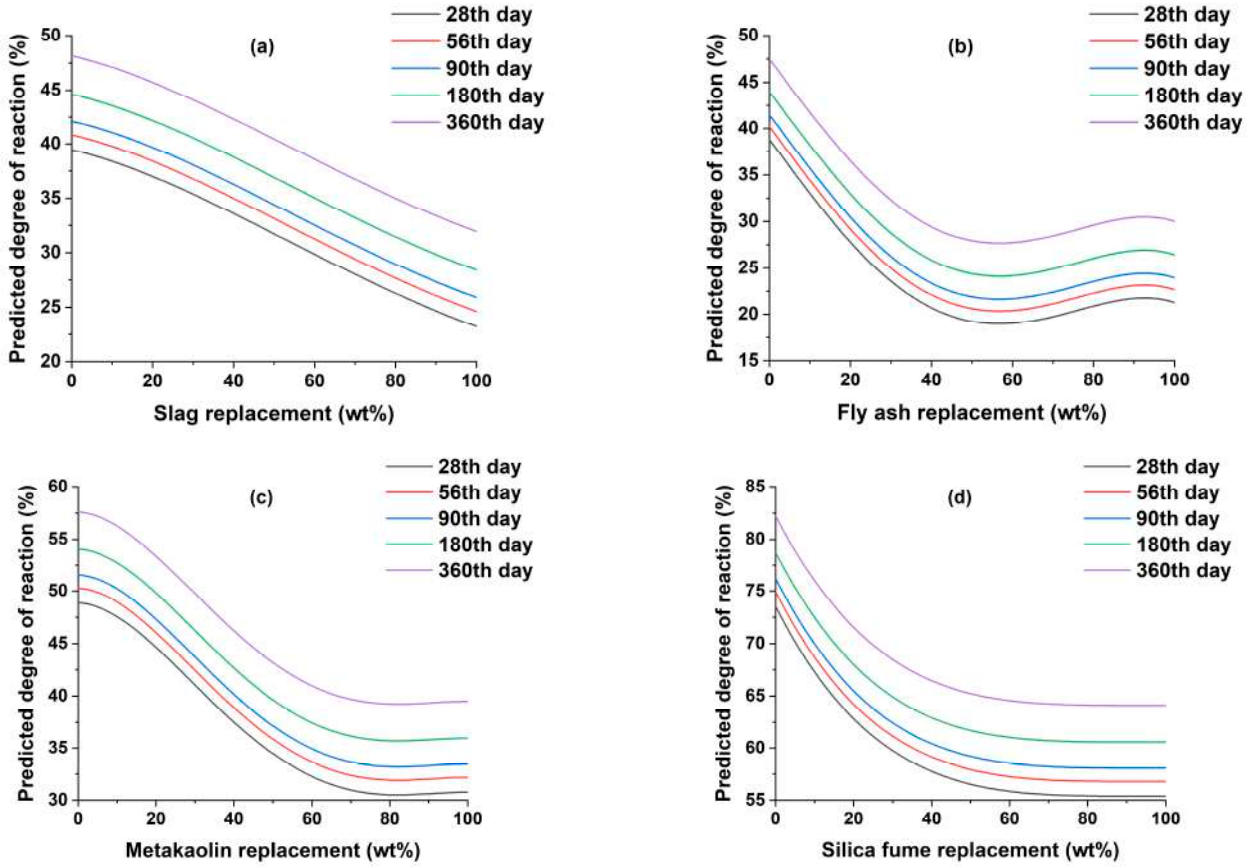

Figure 3. The effect of curing time on the degree of reaction of (**a**) slag, (**b**) fly ash, (**c**) metakaolin, and (**d**) silica fume.

The effect of the chemical composition of SCMs on the DOR is shown in Figure 4. The chemistry of the SCMs was characterized by their major oxide percentage compositions, which are Ca-Si-Al for slag, Si-Al for fly ash and metakaolin, and Si for silica fume [10]. For all slag replacement ratios, maximum DOR is attained when the wt% composition of the three major oxides is nearly equivalent. As the amount of slag replacement increases, the CaO tends to be surplus, and the system (PC + Slag) starts to intake higher amounts of SiO_2 and Al_2O_3 to increase DOR. This is due to the excess $Ca(OH)_2$ from cement hydration, which can combine with the silica and aluminate of slag to form calcium silicate hydrate (C-S-H) and calcium aluminate hydrate (C-A-H) [66,67].

The effect of the SiO_2/Al_2O_3 ratio of fly ash and metakaolin on the DOR is shown in Figure 5. The SiO_2/Al_2O_3 ratio in fly ash affects the DOR differently depending on the replacement percentage; for example, increasing the silica to alumina ratio lowers the DOR at 10% replacement, nearly has no effect at 30% replacement, and rises at 50% and 70% replacements, respectively. The DOR of metakaolin is highly dependent on the amount of Al_2O_3 content. For all metakaolin replacement levels, the DOR increases with increasing aluminate content. Additionally, the rate of change of DOR becomes more stable due to changes in the SiO_2/Al_2O_3 ratio as the amount of metakaolin replacement increases. This can be supported by the fact that the optimum content for replacing PC with metakaolin ranges from 10–30% [64,68], with further substitution resulting in the creation of excess inert material. Therefore, for higher replacement levels, changes in metakaolin oxide composition have little effect on the DOR. However, it is essential to emphasize that the SiO_2/Al_2O_3 ratio variations are contingent upon the specific cementitious composition. For instance, Juengsuwattananon et al. [69] observed that the DOR increases to a SiO_2/Al_2O_3 ratio of up to 4 in geopolymer compositions containing metakaolin and rice husk ash. Yet, further increment results in reduced DOR. In another study, Duxson et al. [70] found that

in geopolymer formulations comprising metakaolin and an alkaline silicate solution, the DOR tends to increase up to a SiO_2/Al_2O_3 ratio of 1.9, but samples with a SiO_2/Al_2O_3 ratio of 2.15 displayed lower levels of DOR.

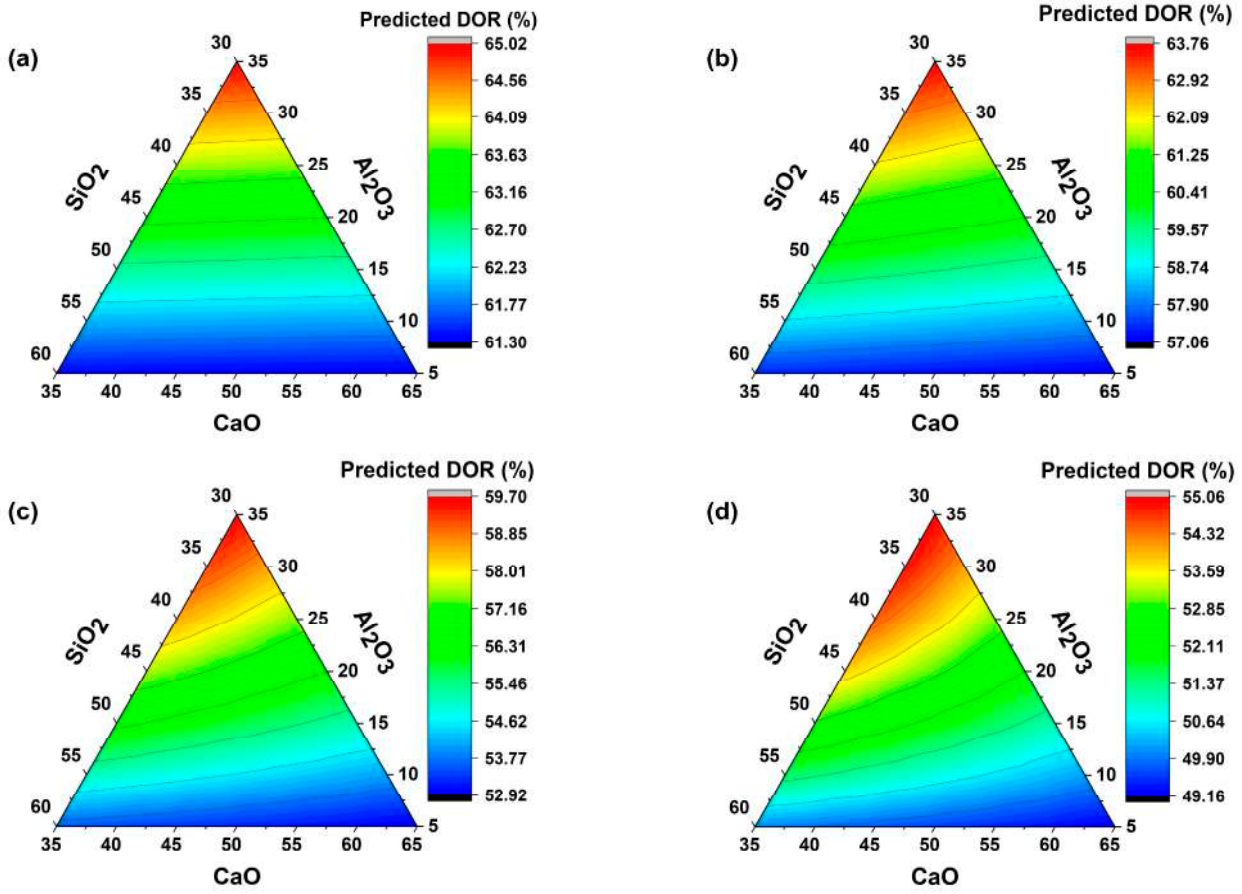

Figure 4. Effect of (**a**) 10% slag replacement, (**b**) 30% slag replacement, (**c**) 50% slag replacement, and (**d**) 70% slag replacement oxide composition on the degree of reaction.

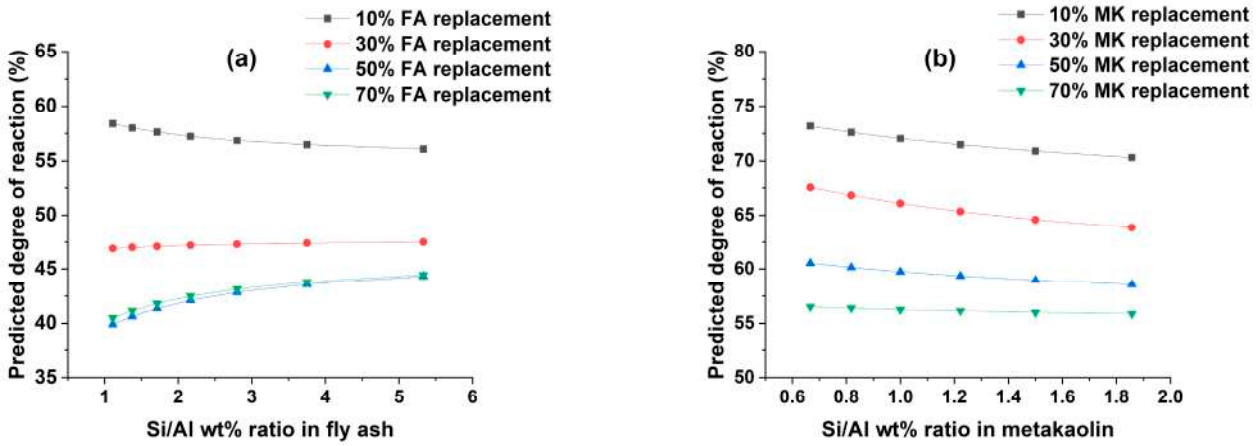

Figure 5. Effect of SiO_2/Al_2O_3 ratio on the degree of reaction of (**a**) fly ash and (**b**) metakaolin.

The effect of SiO_2 content in silica fume on the DOR is shown in Figure 6. According to ASTM C 1240 [71], the minimum SiO_2 content for silica fume must be 85%. Additionally, the average SiO_2 content of the collected silica fume samples is greater than 95%; hence, the DOR variation was checked for SiO_2 content ranging from 90 to 100%. The result indicates

the DOR of silica fume remains constant due to changes in SiO_2 content in the specified range. The same observations were reported previously [72].

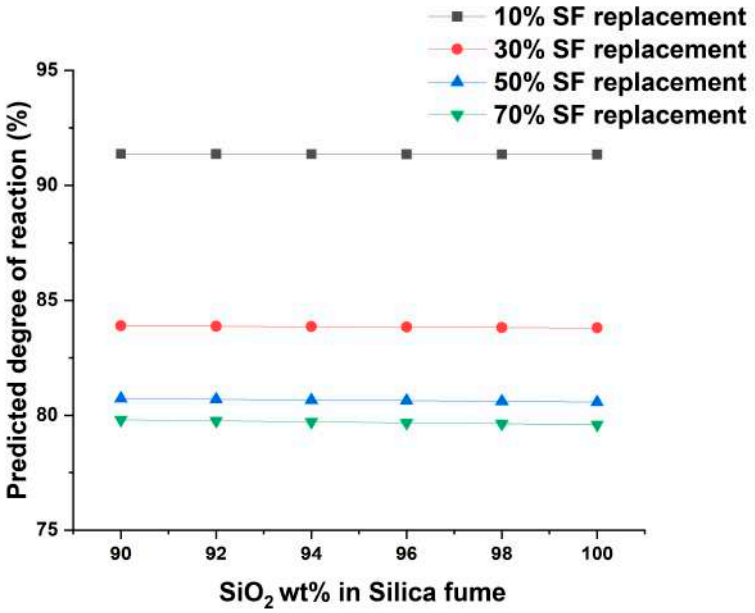

Figure 6. Effect of SiO_2 on the degree of reaction of silica fume.

These correlations, in addition to the noted proximity of the prediction of the model to experimental data, can support the accuracy of the model by aligning with findings from previous studies. This underscores consistent trends in DOR concerning various input parameters and, in turn, reinforces the reliability and applicability of the model. Moreover, comparisons between the predicted DOR trends and phase assemblage outputs further validate the model, especially in scenarios where replacement levels have not been thoroughly investigated in previous studies. The insights gained from this model significantly contribute to understanding how diverse input parameters influence the DOR of SCMs, further establishing the suitability of the model.

4. Predicted Phase Assemblages

4.1. PC–Slag

The thermodynamic modeling results of PC blended with slag is shown in Figure 7a. The initial phases of PC–slag (100% PC) are hydrogarnet, C-(A)-S-H, ettringite, monosulfate, and portlandite. As the level of slag replacement increases, the volumes of unreacted PC and hydrogarnet decrease while the volume of unreacted slag and hydrotalcite increases. The volume of C-(A)-S-H slightly increases up to 80% slag replacement. After this point, there is a slight decrease in the volume of C-(A)-S-H, while more ettringite is expected to form. This slag replacement level also coincides with the complete consumption of portlandite. Monosulfate remains constant for the majority of slag replacement, while it is not a stable phase at >88% slag. The volume of total hydrates formed generally reduces as the slag replacement increases. Lothenbach et al. [73] performed thermodynamic calculations for PC–slag systems, assuming full hydration of PC and 75% DOR of the slag, which almost yielded equivalent results except for the formation of Fe-hydrogarnet, which was not considered due to its slow kinetics of formation, and the formation of monosulfate in place of monocarbonate, due to the higher sulfate content in the slag used in the simulation. On the other hand, a similar result is reported in a study by Park et al. [74].

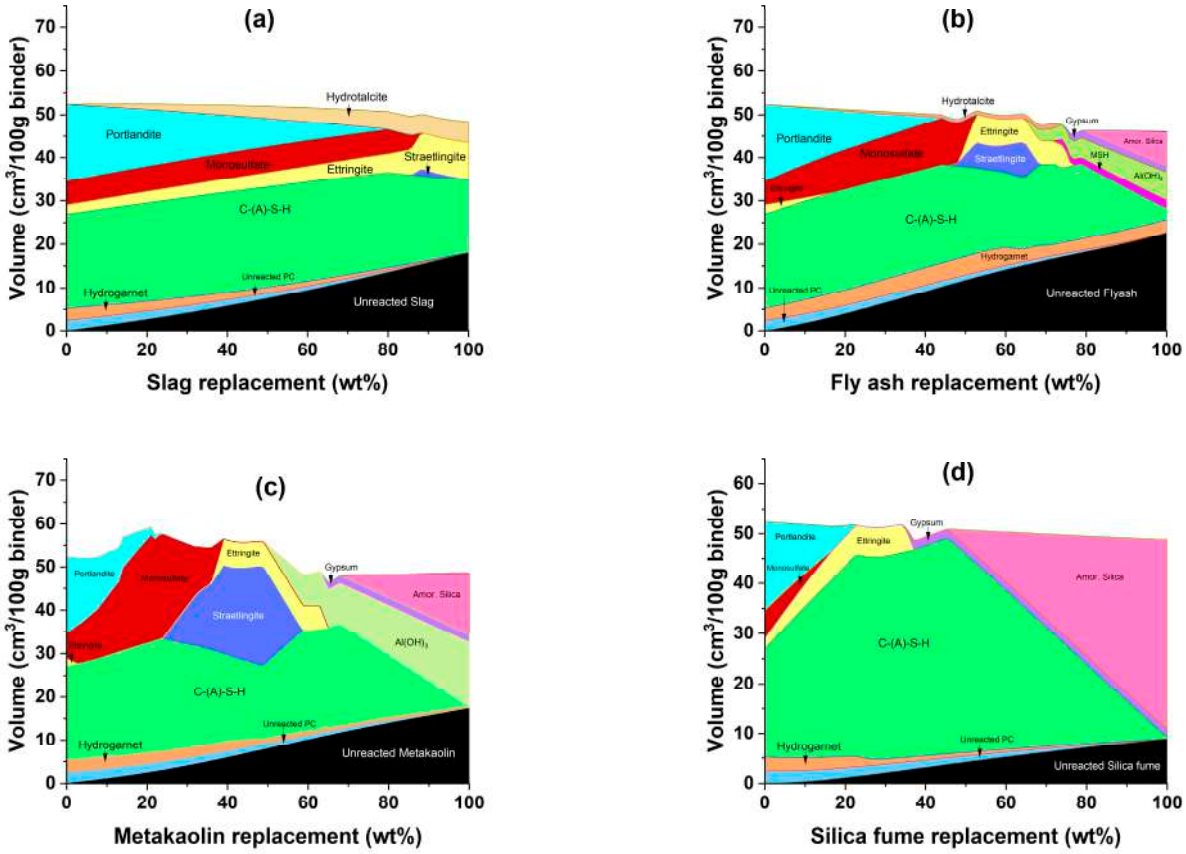

Figure 7. Simulated phase assemblage of hydration of Portland cement with incremental replacement of (**a**) slag, (**b**) fly ash, (**c**) metakaolin, and (**d**) silica fume.

4.2. PC–Fly Ash

The thermodynamic modeling results of PC blended with fly ash are shown in Figure 7b. As the level of fly ash replacement increases, unreacted PC, unreacted fly ash, and hydrotalcite follow the same trends as PC–slag systems, except for hydrogarnet, which remains constant and exhibits greater volumes due to the higher ferrite content of fly ash compared to slag. The volume of C-(A)-S-H slightly increases up to 45% fly ash replacement. Following this point, the volume of C-(A)-S-H decreases slightly, while more straetlingite, $Al(OH)_3$, and amorphous silica are expected to form. This fly ash replacement level also coincides with the complete consumption of portlandite but with a faster rate of destabilization compared to slag. This is supported by the presence of additional aluminate in fly ash, which leads to a pozzolanic reaction whereby portlandite reacts with aluminate to form additional C-A-H [75]. A higher concentration of SiO_2 and Al_2O_3 also resulted in the formation of $Al(OH)_3$ and amorphous silica. The volume of monosulfate increases until it is completely degraded into ettringite, which eventually degrades to form gypsum. The volume of hydrotalcite slightly increases until it is destabilized into M-S-H, however, these phases are found in smaller volumes indicating lower magnesia content of fly ash. The volume of total hydrates formed generally reduces as fly ash replacement increases. The main difference between this research and prior works [73,76] is the formation of M-S-H, amorphous silica, and higher volumes of $Al(OH)_3$, which is due to excess SiO_2 and Al_2O_3 in the system. This point is further supported by the significant drop in DOR of fly ash as the replacement of PC with fly ash increases.

4.3. PC–Metakaolin

The thermodynamic modeling results of PC blended with metakaolin are shown in Figure 7c. Unreacted PC, unreacted metakaolin, and hydrogarnet follow the same trends

as PC–slag systems when the quantity of metakaolin replacement increases. The volume of C-(A)-S-H increases up to 23% metakaolin replacement. This metakaolin replacement level also coincides with the complete consumption of portlandite. Portlandite is consumed faster than both PC–slag and PC–fly ash systems [37]. From this point up to 60% MK replacement, C-(A)-S-H begins to deteriorate and then increases, primarily to accommodate the formation of straetlingite, after which it gradually degrades into $Al(OH)_3$ and amorphous silica. Straetlingite is formed from the decomposition of C-(A)-S-H and monosulfate [77]. The formation of straetlingite is associated with an increase in the volume of total hydrates formed, which is also true for slag and fly ash replacements, albeit in smaller amounts. The volume of monosulfate increases until it is completely degraded into ettringite, which eventually degrades to form gypsum. Due to the extra SiO_2 and Al_2O_3 oxide composition of metakaolin, the volumes of straetlingite, $Al(OH)_3$, and amorphous silica are greater than in PC–slag and PC–fly ash systems. The volume of total hydrates formed reduced in the same manner as it did in the PC–slag and PC–fly ash systems.

4.4. PC–Silica Fume

The thermodynamic modeling results of PC blended with silica fume is shown in Figure 7d. Silica fume is mainly composed of SiO_2. As the level of silica fume replacement increases, unreacted PC, unreacted silica fume, and hydrogarnet follow the same trends as in PC–metakaolin systems. The volume of C-(A)-S-H increases up to 45% silica fume replacement. After this point, the volume of C-(A)-S-H declines, while amorphous silica starts to form. This silica fume replacement level also coincides with the complete consumption of portlandite. Portlandite is consumed faster than both PC–slag and PC–fly ash systems but in a nearly equal amount to the PC–Metakaolin system. The volume of monosulfate decreases until it is completely degraded into ettringite, which eventually degrades to form gypsum. Despite being relatively small, the volume of total hydrates formed reduced as silica fume replacement increased, as it did with the other SCMs [73].

5. Conclusions

This study proposed a means of determining the DOR of SCMs in hydrated Portland cement by adapting a machine learning algorithm. The following conclusions were drawn from the obtained results:

- The model exhibited satisfactory performance for predicting the DOR of SCMs, achieving an average accuracy of 89% and a minimum accuracy of 83%. These findings establish a solid foundation for predicting DOR and analyzing diverse DOR-related relationships in SCMs, encompassing different known or unknown properties, particularly in the case of new materials.
- For all SCMs, the DOR increases with increasing w/c ratios and curing time and decreases with replacement ratios.
- The DOR of SCMs is predicted to exhibit significant changes based on oxide composition. For instance, slag with higher Al_2O_3 content is expected to show higher levels of DOR, while the DOR of metakaolin show less extent of change despite the variations in the Si/Al ratio of metakaolin.
- The proposed model will be highly useful for simulating phase assemblages of SCM-blended PC, as it provides a reasonable basis for predicting the DOR of SCMs covering numerous parameters related to material properties and curing conditions when no experimental data are available.

Author Contributions: Conceptualization, A.B.D., B.Y. and S.P. (Solmoi Park); Formal analysis, A.B.D., B.Y. and S.P. (Solmoi Park); Investigation, A.B.D., S.P. (Seunghee Park), B.Y. and S.P. (Solmoi Park); Methodology, A.B.D., S.P. (Seunghee Park), B.Y. and S.P. (Solmoi Park); Software, S.P. (Solmoi Park); Supervision, S.P. (Solmoi Park); Validation, B.Y.; Writing—original draft, A.B.D.; Writing—review and editing, S.P. (Seunghee Park), B.Y. and S.P. (Solmoi Park). All authors have read and agreed to the published version of the manuscript.

Funding: This work was supported by the National Research Foundation of Korea (NRF) grant funded by the Korea government (MSIT) (No. 2021R1A4A3033128, 2020R1C1C1005063 and 2022R1C1C1007498).

Institutional Review Board Statement: Not applicable.

Informed Consent Statement: Not applicable.

Data Availability Statement: The data presented in this study are available on request from the corresponding author.

Conflicts of Interest: The authors declare no conflict of interest.

References

1. Scrivener, K.L.; John, V.M.; Gartner, E.M. Eco-Efficient Cements: Potential Economically Viable Solutions for a Low-CO_2 Cement-Based Materials Industry. *Cem. Concr. Res.* **2018**, *114*, 2–26. [CrossRef]
2. Cormos, C.-C. Decarbonization Options for Cement Production Process: A Techno-Economic and Environmental Evaluation. *Fuel* **2022**, *320*, 123907. [CrossRef]
3. Wei, J.; Cen, K.; Geng, Y. China's Cement Demand and CO_2 Emissions toward 2030: From the Perspective of Socioeconomic, Technology and Population. *Environ. Sci. Pollut. Res.* **2019**, *26*, 6409–6423. [CrossRef] [PubMed]
4. Tam, C.; Taylor, M.; Gielen, D.; Twigg, C.; Klee, H.; Rocha, P.; Meer, R.v.d. Cement Technology Roadmap 2009—Carbon Emissions Reductions Up to 2050. Available online: https://www.iea.org/reports/cement-technology-roadmap-carbon-emissions-reductions-up-to-2050 (accessed on 1 July 2022).
5. Vass, T.; Levi, P.; Gouy, A.; Mandová, H. *Cement*; IEA: Paris, French, 2021.
6. Coffetti, D.; Crotti, E.; Gazzaniga, G.; Carrara, M.; Pastore, T.; Coppola, L. Pathways towards Sustainable Concrete. *Cem. Concr. Res.* **2022**, *154*, 106718. [CrossRef]
7. Juenger, M.C.G.; Snellings, R.; Bernal, S.A. Supplementary Cementitious Materials: New Sources, Characterization, and Performance Insights. *Cem. Concr. Res.* **2019**, *122*, 257–273. [CrossRef]
8. Schneider, M. The Cement Industry on the Way to a Low-Carbon Future. *Cem. Concr. Res.* **2019**, *124*, 105792. [CrossRef]
9. Pacewska, B.; Wilińska, I. Usage of Supplementary Cementitious Materials: Advantages and Limitations: Part I. C–S–H, C–A–S–H and Other Products Formed in Different Binding Mixtures. *J. Therm. Anal. Calorim.* **2020**, *142*, 371–393. [CrossRef]
10. Snellings, R. Assessing, Understanding and Unlocking Supplementary Cementitious Materials. *RILEM Tech. Lett.* **2016**, *1*, 50. [CrossRef]
11. Moon, G.D.; Oh, S.; Jung, S.H.; Choi, Y.C. Effects of the Fineness of Limestone Powder and Cement on the Hydration and Strength Development of PLC Concrete. *Constr. Build. Mater.* **2017**, *135*, 129–136. [CrossRef]
12. Scrivener, K.; Martirena, F.; Bishnoi, S.; Maity, S. Calcined Clay Limestone Cements (LC3). *Cem. Concr. Res.* **2018**, *114*, 49–56. [CrossRef]
13. Bullard, J.W.; Garboczi, E.J.; Stutzman, P.E.; Feng, P.; Brand, A.S.; Perry, L.K.; Hagedorn, J.; Griffin, W.; Terrill, J.E. Measurement and Modeling Needs for Microstructure and Reactivity of Next-Generation Concrete Binders. *Cem. Concr. Compos.* **2019**, *101*, 24–31. [CrossRef]
14. Choi, T. Bayesian Regression with Gaussian Processes: A Tutorial. In Proceedings of the Spring Conference, Hong Kong, 23–25 May 2011; The Korean Statistical Society: Seoul, Republic of Korea; pp. 77–81.
15. Li, Z.; Yoon, J.; Zhang, R.; Rajabipour, F.; Srubar, W.V., III; Dabo, I.; Radlińska, A. Machine Learning in Concrete Science: Applications, Challenges, and Best Practices. *NPJ Comput. Mater.* **2022**, *8*, 127. [CrossRef]
16. Ahmad, W.; Ahmad, A.; Ostrowski, K.A.; Aslam, F.; Joyklad, P.; Zajdel, P. Application of Advanced Machine Learning Approaches to Predict the Compressive Strength of Concrete Containing Supplementary Cementitious Materials. *Materials* **2021**, *14*, 5762. [CrossRef]
17. Quan Tran, V. Machine Learning Approach for Investigating Chloride Diffusion Coefficient of Concrete Containing Supplementary Cementitious Materials. *Constr. Build. Mater.* **2022**, *328*, 127103. [CrossRef]
18. Rahla, K.M.; Mateus, R.; Bragança, L. Comparative Sustainability Assessment of Binary Blended Concretes Using Supplementary Cementitious Materials (SCMs) and Ordinary Portland Cement (OPC). *J. Clean. Prod.* **2019**, *220*, 445–459. [CrossRef]
19. Shah, H.A.; Yuan, Q.; Photwichai, N. Use of Materials to Lower the Cost of Ultra-High-Performance Concrete—A Review. *Constr. Build. Mater.* **2022**, *327*, 127045. [CrossRef]

20. Hossain, M.U.; Poon, C.S.; Dong, Y.H.; Xuan, D. Evaluation of Environmental Impact Distribution Methods for Supplementary Cementitious Materials. *Renew. Sustain. Energy Rev.* **2018**, *82*, 597–608. [CrossRef]
21. Wei, C.; Yan, Y.; Zhang, Z.; Liu, X.; Wu, P.; Gu, J.; Han, F.; Ren, Q. Insight into the Synergic Effects of Circulating Fluidized Bed Fly Ash, Red Mud and Blast Furnace Slag in Preparation of Ultrahigh-Performance Concrete: Reaction Mechanism and Performance Optimization. *Constr. Build. Mater.* **2023**, *403*, 133120. [CrossRef]
22. Tushar, Q.; Bhuiyan, M.A.; Zhang, G.; Maqsood, T.; Tasmin, T. Application of a Harmonized Life Cycle Assessment Method for Supplementary Cementitious Materials in Structural Concrete. *Constr. Build. Mater.* **2022**, *316*, 125850. [CrossRef]
23. Siddika, A.; Al Mamun, M.A.; Alyousef, R.; Mohammadhosseini, H. State-of-the-Art-Review on Rice Husk Ash: A Supplementary Cementitious Material in Concrete. *J. King Saud Univ. Eng. Sci.* **2021**, *33*, 294–307. [CrossRef]
24. Searson, D. GPTIPS Symbolic Data Mining Platform for MATLAB. 2014. Available online: https://sites.google.com/site/gptips4matlab/ (accessed on 1 July 2022).
25. Ben Haha, M.; De Weerdt, K.; Lothenbach, B. Quantification of the Degree of Reaction of Fly Ash. *Cem. Concr. Res.* **2010**, *40*, 1620–1629. [CrossRef]
26. Kocaba, V.; Gallucci, E.; Scrivener, K.L. Methods for Determination of Degree of Reaction of Slag in Blended Cement Pastes. *Cem. Concr. Res.* **2012**, *42*, 511–525. [CrossRef]
27. Scrivener, K.L.; Lothenbach, B.; De Belie, N.; Gruyaert, E.; Skibsted, J.; Snellings, R.; Vollpracht, A. TC 238-SCM: Hydration and Microstructure of Concrete with SCMs: State of the Art on Methods to Determine Degree of Reaction of SCMs. *Mater. Struct. Constr.* **2015**, *48*, 835–862. [CrossRef]
28. Durdziński, P.T.; Ben Haha, M.; Bernal, S.A.; De Belie, N.; Gruyaert, E.; Lothenbach, B.; Menéndez Méndez, E.; Provis, J.L.; Schöler, A.; Stabler, C.; et al. Outcomes of the RILEM Round Robin on Degree of Reaction of Slag and Fly Ash in Blended Cements. *Mater. Struct. Constr.* **2017**, *50*, 135. [CrossRef]
29. Kang, H.; Lee, N.; Moon, J. Elucidation of the Hydration Reaction of Uhpc Using the Ponkcs Method. *Materials* **2020**, *13*, 4661. [CrossRef]
30. Pfingsten, J.; Rickert, J.; Lipus, K. Estimation of the Content of Ground Granulated Blast Furnace Slag and Different Pozzolanas in Hardened Concrete. *Constr. Build. Mater.* **2018**, *165*, 931–938. [CrossRef]
31. Li, L.; Yang, J.; Shen, X. Measuring the Hydration Product Proportion in Composite Cement Paste by Using Quantitative BSE-EDS Image Analysis: A Comparative Study. *Measurement* **2022**, *19*, 111290. [CrossRef]
32. Walkley, B.; Provis, J.L. Solid-State Nuclear Magnetic Resonance Spectroscopy of Cements. *Mater. Today Adv.* **2019**, *1*, 100007. [CrossRef]
33. Polenova, T.; Gupta, R.; Goldbourt, A. Magic Angle Spinning NMR Spectroscopy: A Versatile Technique for Structural and Dynamic Analysis of Solid-Phase Systems. *Anal. Chem.* **2015**, *87*, 5458–5469. [CrossRef]
34. Ferraz, E.; Andrejkovičová, S.; Hajjaji, W.; Velosa, A.L.; Silva, A.S.; Rocha, F. Pozzolanic Activity of Metakaolins by the French Standard of the Modified Chapelle Test: A Direct Methodology. *Acta Geodyn. Geomater.* **2015**, *12*, 289–298. [CrossRef]
35. Quarcioni, V.A.; Chotoli, F.F.; Coelho, A.C.V.; Cincotto, M.A. Indirect and Direct Chapelle's Methods for the Determination of Lime Consumption in Pozzolanic Materials Métodos de Ensaio Indiretos e Método Chapelle Direto Para Determinação Do Consumo de Cal Pelos Materiais Pozolânicos. *Rev. Ibracon Estrut. Mater.* **2015**, *8*, 1–7. [CrossRef]
36. Snellings, R.; Scrivener, K.L. Rapid Screening Tests for Supplementary Cementitious Materials: Past and Future. *Mater. Struct. Constr.* **2016**, *49*, 3265–3279. [CrossRef]
37. Donatello, S.; Tyrer, M.; Cheeseman, C.R. Comparison of Test Methods to Assess Pozzolanic Activity. *Cem. Concr. Compos.* **2010**, *32*, 121–127. [CrossRef]
38. *BS EN 196-5*; BSI Standards Publication Methods of Testing Cement Part 5: Pozzolanicity Test for Pozzolanic Cement. European Standard; BSI Publications: London, UK, 2011.
39. Tironi, A.; Trezza, M.A.; Scian, A.N.; Irassar, E.F. Assessment of Pozzolanic Activity of Different Calcined Clays. *Cem. Concr. Compos.* **2013**, *37*, 319–327. [CrossRef]
40. Wang, Y.; Burris, L.; Shearer, C.R.; Hooton, D.; Suraneni, P. Strength Activity Index and Bulk Resistivity Index Modifications That Differentiate Inert and Reactive Materials. *Cem. Concr. Compos.* **2021**, *124*, 104240. [CrossRef]
41. Ramanathan, S.; Pestana, L.R.; Suraneni, P. Reaction Kinetics of Supplementary Cementitious Materials in Reactivity Tests. *Cement* **2022**, *8*, 100022. [CrossRef]
42. Narmluk, M.; Nawa, T. Effect of Fly Ash on the Kinetics of Portland Cement Hydration at Different Curing Temperatures. *Cem. Concr. Res.* **2011**, *41*, 579–589. [CrossRef]
43. Gandomi, A.H.; Atefi, E. Software Review: The GPTIPS Platform. *Genet. Program. Evolvable Mach.* **2020**, *21*, 273–280. [CrossRef]
44. Dagli, C.H. Natural Selection of Asphalt Mix Stiffness Predictive Models with Genetic Programming. *Intell. Eng. Syst. Artif. Neural Netw.* **2010**, *20*, 389–396. [CrossRef]
45. Aquino, H.L.; Concepcion, R.S.; Mayol, A.P.; Bandala, A.A.; Culaba, A.; Cuello, J.; Dadios, E.P.; Ubando, A.T.; San Juan, J.L.G. Prediction of Moisture Content of Chlorella Vulgaris Microalgae Using Hybrid Evolutionary Computing and Neural Network Variants for Biofuel Production. In Proceedings of the 2021 IEEE 13th International Conference on Humanoid, Nanotechnology, Information Technology, Communication and Control, Environment, and Management (HNICEM 2021), Virtual, 28–30 November 2021; pp. 1–6. [CrossRef]

46. Shin, Y.; Park, H.M.; Park, J.; Cho, H.; Oh, S.E.; Chung, S.Y.; Yang, B. Effect of Polymer Binder on the Mechanical and Microstructural Properties of Pervious Pavement Materials. *Constr. Build. Mater.* **2022**, *325*, 126209. [CrossRef]
47. Wagner, T.; Kulik, D.A.; Hingerl, F.F.; Dmytrievava, S.V. Gem-Selektor Geochemical Modeling Package: TSolMod Library and Data Interface for Multicomponent Phase Models. *Can. Mineral.* **2012**, *50*, 1173–1195. [CrossRef]
48. Kulik, D.A.; Wagner, T.; Dmytrieva, S.V.; Kosakowski, G.; Hingerl, F.F.; Chudnenko, K.V.; Berner, U.R. GEM-Selektor Geochemical Modeling Package: Revised Algorithm and GEMS3K Numerical Kernel for Coupled Simulation Codes. *Comput. Geosci.* **2013**, *17*, 1–24. [CrossRef]
49. Lothenbach, B.; Kulik, D.A.; Matschei, T.; Balonis, M.; Baquerizo, L.; Dilnesa, B.; Miron, G.D.; Myers, R.J. Cemdata18: A Chemical Thermodynamic Database for Hydrated Portland Cements and Alkali-Activated Materials. *Cem. Concr. Res.* **2019**, *115*, 472–506. [CrossRef]
50. Helgeson, H.C.; Kirkham, D.H.; Flowers, G.C. Theoretical Prediction of the Thermodynamic Behavior of Aqueous Electrolytes at High Pressures and Temperatures: IV. Calculation of Activity Coefficients, Osmotic Coefficients, and Apparent Molal and Standard and Relative Partial Molal Properties to 600 °C. *Am. J. Sci.* **1981**, *281*, 1249–1516. [CrossRef]
51. Lothenbach, B.; Winnefeld, F. Thermodynamic Modelling of the Hydration of Portland Cement. *Cem. Concr. Res.* **2006**, *36*, 209–226. [CrossRef]
52. Lothenbach, B.; Matschei, T.; Möschner, G.; Glasser, F.P. Thermodynamic Modelling of the Effect of Temperature on the Hydration and Porosity of Portland Cement. *Cem. Concr. Res.* **2008**, *38*, 1–18. [CrossRef]
53. Parrot, L.J.; Killoh, D.C. Prediction of Cement Hydration. *Br. Ceram. Proc.* **1984**, *35*, 41–53.
54. Ke, X.; Bernal, S.A.; Provis, J.L.; Lothenbach, B. Thermodynamic Modelling of Phase Evolution in Alkali-Activated Slag Cements Exposed to Carbon Dioxide. *Cem. Concr. Res.* **2020**, *136*, 106158. [CrossRef]
55. Reddy, V.M.; Rao, D.M.V.S. Effect of w/c Ratio on Workability and Mechanical Properties of High Strength Self Compacting Concrete (M70 Grade). *IOSR J. Mech. Civ. Eng.* **2014**, *11*, 15–21. [CrossRef]
56. Lothenbach, B.; Le Saout, G.; Ben Haha, M.; Figi, R.; Wieland, E. Hydration of a Low-Alkali CEM III/B-SiO 2 Cement (LAC). *Cem. Concr. Res.* **2012**, *42*, 410–423. [CrossRef]
57. Snellings, R.; Machner, A.; Bolte, G.; Kamyab, H.; Durdzinski, P.; Teck, P.; Zajac, M.; Muller, A.; de Weerdt, K.; Haha, M. Ben Hydration Kinetics of Ternary Slag-Limestone Cements: Impact of Water to Binder Ratio and Curing Temperature. *Cem. Concr. Res.* **2022**, *151*, 106647. [CrossRef]
58. Escalante, J.I.; Gómez, L.Y.; Johal, K.K.; Mendoza, G.; Mancha, H.; Méndez, J. Reactivity of Blast-Furnace Slag in Portland Cement Blends Hydrated under Different Conditions. *Cem. Concr. Res.* **2001**, *31*, 1403–1409. [CrossRef]
59. Snellings, R.; Kazemi-Kamyab, H.; Nielsen, P.; Van den Abeele, L. Classification and Milling Increase Fly Ash Pozzolanic Reactivity. *Front. Built Environ.* **2021**, *7*, 670996. [CrossRef]
60. Zhang, G.; Wei, Q.; Ding, Q.; Wang, A.; Liu, K. Effect of Curing Temperature and Fly Ash Content on the Hydration and Microstructure of Fly Ash–Cement Pastes. *J. Sustain. Cem. Mater.* **2018**, *7*, 372–383. [CrossRef]
61. Zhao, D.; Khoshnazar, R. Microstructure of Cement Paste Incorporating High Volume of Low-Grade Metakaolin. *Cem. Concr. Compos.* **2020**, *106*, 103453. [CrossRef]
62. Wei, Y.; Yao, W.; Xing, X.; Wu, M. Quantitative Evaluation of Hydrated Cement Modified by Silica Fume Using QXRD, 27Al MAS NMR, TG-DSC and Selective Dissolution Techniques. *Constr. Build. Mater.* **2012**, *36*, 925–932. [CrossRef]
63. Uzbas, B.; Aydin, A.C. Microstructural Analysis of Silica Fume Concrete with Scanning Electron Microscopy and X-Ray Diffraction. *Eng. Technol. Appl. Sci. Res.* **2020**, *10*, 5845–5850. [CrossRef]
64. Wei, J.; Gencturk, B. Hydration of Ternary Portland Cement Blends Containing Metakaolin and Sodium Bentonite. *Cem. Concr. Res.* **2019**, *123*, 105772. [CrossRef]
65. Whittaker, M.; Zajac, M.; Ben Haha, M.; Bullerjahn, F.; Black, L. The Role of the Alumina Content of Slag, plus the Presence of Additional Sulfate on the Hydration and Microstructure of Portland Cement-Slag Blends. *Cem. Concr. Res.* **2014**, *66*, 91–101. [CrossRef]
66. Wang, S.D.; Scrivener, K.L. Hydration Products of Alkali Activated Slag Cement. *Cem. Concr. Res.* **1995**, *25*, 561–571. [CrossRef]
67. Mozgawa, W.; Deja, J. Spectroscopic Studies of Alkaline Activated Slag Geopolymers. *J. Mol. Struct.* **2009**, *924–926*, 434–441. [CrossRef]
68. Kocak, Y. Effects of Metakaolin on the Hydration Development of Portland–Composite Cement. *J. Build. Eng.* **2020**, *31*, 101419. [CrossRef]
69. Juengsuwattananon, K.; Winnefeld, F.; Chindaprasirt, P.; Pimraksa, K. Correlation between Initial SiO_2/Al_2O_3, Na_2O/Al_2O_3, Na_2O/SiO_2 and H_2O/Na_2O Ratios on Phase and Microstructure of Reaction Products of Metakaolin-Rice Husk Ash Geopolymer. *Constr. Build. Mater.* **2019**, *226*, 406–417. [CrossRef]
70. Duxson, P.; Provis, J.L.; Lukey, G.C.; Mallicoat, S.W.; Kriven, W.M.; Van Deventer, J.S.J. Understanding the Relationship between Geopolymer Composition, Microstructure and Mechanical Properties. *Colloids Surf. A Physicochem. Eng. Asp.* **2005**, *269*, 47–58. [CrossRef]
71. ASTM International. ASTM C 1240 Standard Specification for Silica Fume Used in Cementitious Mixtures. *Annu. B. ASTM Stand.* **2003**, *15*, 1–6.
72. Wolsiefer, J.; Sivasundaram, V.; Malhotra, V.M.; Carette, G.C. Performance of Concretes Incorporating Various Forms of Silica Fume. *Am. Concr. Inst. ACI Spec. Publ.* **1995**, *SP-153*, 591–655.

73. Lothenbach, B.; Scrivener, K.; Hooton, R.D. Supplementary Cementitious Materials. *Cem. Concr. Res.* **2011**, *41*, 1244–1256. [CrossRef]
74. Park, K.B.; Wang, Y.S.; Wang, X.Y. Property Analysis of Slag Composite Concrete Using a Kinetic–Thermodynamic Hydration Model. *Appl. Sci.* **2021**, *11*, 7191. [CrossRef]
75. Papadakis, V.G. Effect of Fly Ash on Portland Cement Systems: Part I. Low-Calcium Fly Ash. *Cem. Concr. Res.* **1999**, *29*, 1727–1736. [CrossRef]
76. Durdziński, P.T.; Ben Haha, M.; Zajac, M.; Scrivener, K.L. Phase Assemblage of Composite Cements. *Cem. Concr. Res.* **2017**, *99*, 172–182. [CrossRef]
77. Kunther, W.; Dai, Z.; Skibsted, J. Thermodynamic Modeling of Hydrated White Portland Cement-Metakaolin-Limestone Blends Utilizing Hydration Kinetics from 29Si MAS NMR Spectroscopy. *Cem. Concr. Res.* **2016**, *86*, 29–41. [CrossRef]